Proc. Natl. Acad. Sci. USA
Vol. 89, pp. 6114–6118, July 1992
Biochemistry

Structures of apo and complexed *Escherichia coli* glycinamide ribonucleotide transformylase

ROBERT J. ALMASSY, CHERYL A. JANSON, CHEN-CHEN KAN, AND ZUZANA HOSTOMSKA

Agouron Pharmaceuticals, 3565 General Atomics Court, San Diego, CA 92121

Communicated by John Abelson, March 17, 1992

ABSTRACT **The three-dimensional structure of phosphoribosylglycinamide formyltransferase (10-formyltetrahydrofolate:5′-phosphoribosylglycinamide formyltransferase, EC 2.1.2.2) has been solved both as an apoenzyme at 2.8-Å resolution and as a ternary complex with the substrate glycinamide ribonucleotide and a folate inhibitor at 2.5-Å resolution. The structure is a modified doubly wound α/β sheet with flexibility in the active site, including a disordered loop in the apo structure, which is ordered in the ternary complex structure. This enzyme is a target for anti-cancer therapy and now for structure-based drug design.**

The importance of folates in cellular metabolism has been recognized for nearly 50 yr. Derivatives of tetrahydrofolate, carrying single carbon units at various oxidation levels, are used in the biosynthesis of purines, pyrimidines, and amino acids. The first inhibitors of these processes designed as potential antimetabolites of folic acid (aminopterin and methotrexate) blocked dihydrofolate reductase (DHFR), the enzyme responsible for maintaining the folate cofactor in its fully reduced and biologically relevant oxidation state. These compounds and related species-selective inhibitors of DHFR have found widespread clinical use as antineoplastic, antibacterial, and antiprotozoal agents. More recently, as biochemical roles for other folate enzymes have become better understood, enzymes other than DHFR have emerged as attractive targets for additional classes of folate antagonists. Notable among these is phosphoribosylglycinamide formyltransferase (10-formyltetrahydrofolate: 5′-phosphoribosylglycinamide formyltransferase, EC 2.1.2.2, 212 residues, M_r = 23,237; GART), which catalyzes the transfer of a formyl group from 10-formyltetrahydrofolate (10fTHF) to glycinamide ribonucleotide (GAR), a reaction in the purine biosynthetic pathway. An antifolate, 5,10-dideazatetrahydrofolate (1, 2), has been shown to inhibit GART, *de novo* purine biosynthesis, and proliferation of tumor cells in culture (3) and is currently completing phase I clinical trials in a number of centers. This enzyme is, therefore, a good target for anti-cancer therapy and structure-based drug design.

In prokaryotes, GART is found as a single protein but in most eukaryotes it is found as the C-terminal portion of a large multifunctional protein (M_r > 100,000) also containing GAR synthetase and aminoimidazole ribonucleotide synthetase activities. The sequences of GART from prokaryotes and eukaryotes are homologous (4, 5), and the structures are expected to be similar.

Here we report the three-dimensional structure of *Escherichia coli* GART as an apoenzyme (2.8-Å resolution) and also as a ternary complex (2.5-Å resolution) with the substrate GAR and a folate-based inhibitor, 5-deaza-5,6,7,8-tetrahydrofolate (5dTHF) (Fig. 1). The GART structure is a modification of the classic doubly wound α/β sheet with the active site located at the C-terminal edge, near the middle of the seven-

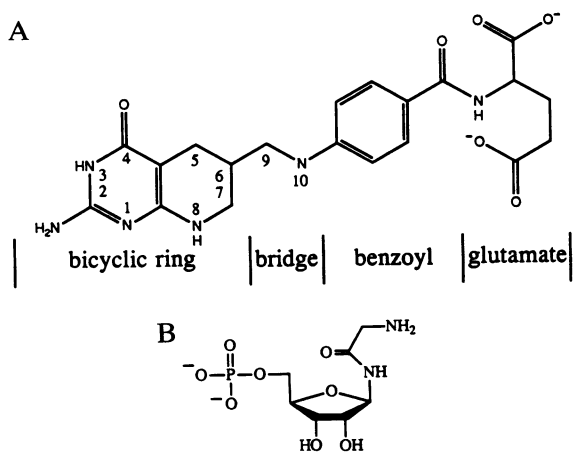

FIG. 1. (*A*) Inhibitor 5dTHF. (*B*) Substrate β-GAR. The coenzyme 10fTHF is identical to 5dTHF, except for NH at the 5 position and a 10-formyl group.

stranded β-sheet. We describe the major changes in the structure between the complexed and uncomplexed forms, interpret structure–activity relationships (SAR), and discuss the mechanism for catalysis based on our structural results.

MATERIALS AND METHODS

The coding region of *E. coli* GART was amplified from *E. coli* K-12 chromosomal DNA with PCR method (6). Primer sequences were derived from *E. coli purN* gene (5). Amplified DNA was confirmed and placed downstream of the T7 bacteriophage gene 10 promoter (7) as the second cistron using modified *E. coli* DHFR translation initiation region as the first cistron (8, 9). The *E. coli* strain AP401-harboring expression plasmid was induced as described (9).

GART was purified by using a DEAE-Sephacel column elution with a 0.03–0.8 M NaCl gradient followed by a Sephadex G75 column and a fast protein liquid chromotography mono Q elution with a 0.03–1 M NaCl gradient. The specific activity of the purified enzyme was 10 μmol/min per mg. All steps were done at 4°C in 50 mM Tris, pH 7.5/30 mM NaCl/1 mM dithiothreitol. A similar purification has since been published (10).

All crystals were grown at 20°C by hanging-drop vapor diffusion. Apo crystals grew from 30 mg of protein per ml in 50 mM Tris (pH 7.5), 1 mM dithiothreitol, and a reservoir of 0.8 M Na^+,K^+ phosphate (pH 6.75) similar to conditions in

The publication costs of this article were defrayed in part by page charge payment. This article must therefore be hereby marked "*advertisement*" in accordance with 18 U.S.C. §1734 solely to indicate this fact.

Abbreviations: GAR, glycinamide ribonucleotide; GART, phosphoribosylglycinamide formyltransferase; DHFR, dihydrofolate reductase; 10fTHF, 10-formyltetrahydrofolate; 5dTHF, 5-deaza-5,6,7,8-tetrahydrofolate; SAR, structure–activity relationships.

*The atomic coordinates and structure factors have been deposited in the Protein Data Bank, Chemistry Department, Brookhaven National Laboratory, Upton, NY 11973 [references: apo structure, 1CDD (coordinates) and 1CDD-SF (structure factors); ternary structure, 1CDE (coordinates) and 1CDE-SF (structure factors)].

ref. 11. Ternary crystals grew from enzyme at 30 mg/ml in the above buffer complexed with GAR and 5dTHF and a reservoir of 154 mM $CaCl_2$/77 mM Mops, pH 7.6/19% (wt/vol) polyethylene glycol 3400/4% (vol/vol) 2-methyl-2,4-pentanediol. The apo structure was solved by isomorphous replacement and solvent leveling from a crystal form with two independent molecules per asymmetric unit (space group $C222_1$, a = 140.9 Å, b = 97.6 Å, c = 102.4 Å), similar to that described by Stura *et al.* (11). Three heavy-atom derivatives used for phasing were prepared by soaking under the following conditions: 1.0 mM MeHgOAc (69 hr), 50% saturated (in water) *cis*-$Pt(NH_3)_2Cl_2$ (33 hr), and 0.5 mM $KAuCl_4$ (25 hr). Heavy-atom positions were initially determined from difference Patterson functions. Two-site solutions were found for MeHgOAc and *cis*-$Pt(NH_3)_2Cl_2$. The heavy-atom model was improved by heavy-atom refinement (12) and double difference Fourier functions. Phases from these derivatives located five sites for the $KAuCl_4$ derivative, with the one major site being consistent with the difference Patterson function (Table 1). Ten cycles of solvent leveling (13) were computed for both a 65% and a 50% solvent content. This computation resulted in a figure of merit, R-factor, phase change, and correlation between $|F_o|$ and $|F_c|$ of 0.81, 24.4%, 31.7°, and 0.964 for the 65% map and 0.82, 23.1%, 29.4°, and 0.967 for the 50% map. A model was built into the density by using the known sequence (5) and computer program FRODO (14). The main-chain connectivity was continuous, except for a disordered loop 110–132. Side-chain density matched the known sequence well. It was found that all 25 heavy-atom-binding sites were located near atoms in residues (histidine, methionine, cysteine) that are potentially reactive toward these heavy atoms, except for two minor sites that may not be real.

The ternary complex (GART, substrate GAR, and inhibitor 5dTHF) was solved by molecular replacement, using the apo-GART model, from a second crystal form (space group $P1$, a = 76.7 Å, b = 72.6 Å, c = 57.0 Å, α = 111.5°, β = 82.8°, γ = 62.6°) with four independent molecules per asymmetric unit. Likely V_m values range from 5.2 to 1.7 $Å^3$/Da, which correspond to two to six molecules per cell. The native Patterson function showed one large peak, 16% of the origin, at ≈(1/2, 0, 1/2). The self-rotation function showed only one large peak (ψ = 50, ϕ = 90, κ = 180), at 61% of the origin. The top two cross rotation function peaks were related by ψ = 49.1, ϕ = 91.2, κ = 174.9. These results suggested there are two dimers in the cell, separated by nearly (1/2, 0, 1/2), with their 2-fold axes approximately parallel. Two monomers were placed at the origin by using the top two cross rotation function Euler angles (5.0, 20.0, 30.0 and 115.0, 95.0, 130.0). The orientations were refined with computer program INTREF (15). A second pair of molecules was then included, at the same initial orientation, and all four orientations were refined.

With these orientations, the translation function clearly showed the intermolecular vectors between the four molecules and resulted in good crystal packing. After additional orientation and position refinement with INTREF, the four-molecule model was refined to an R_{model} of 0.170 (5.0- to 2.8-Å resolution, $F_o > 2\sigma$) with XPLOR (16). The rotations and translations between the molecules were determined by using the known 189 Cα coordinates for each molecule. One averaged model was then refined with XPLOR to an R_{model} of 0.285, enforcing strict noncrystallographic symmetry. The resulting electron density maps were 4-fold averaged. These maps displayed density for parts of the structure not included in the phasing model. Density for the substrate and inhibitor, as well as the 110–132 loop that is disordered in the apocrystal form, became interpretable. Model refinement has started with PROLSQ (17) and XPLOR. The apo models include all protein atoms for residues 1–109 and 133–212, whereas the ternary model includes residues 1–209. The ternary structure is refined as one molecule with strict 4-fold noncrystallographic symmetry transformations. Both apo and ternary models currently include refined individual isotropic temperature factors and no solvent (Table 2).

RESULTS AND DISCUSSION

Structure. The secondary structure of GART is shown in Fig. 2*A*, and the main-chain fold of ternary GART is shown in Fig. 2 *B* and *C*. The primary feature is a central core of smoothly twisting, seven-stranded β-pleated sheet surrounded on both sides by α-helices. The strands of the sheet twist almost 90° from one end of the molecule to the other; the twist has the usual handedness (19).

The fold is a modification of the doubly wound α/β sheet (19). Starting from the N terminus, there is a β–α–β–α–β mononucleotide-binding domain formed from three parallel β-strands connected by two crossover α-helices, a supersecondary structure seen in a variety of proteins (19–21). Succeeding β/α units (β4, α4, and β5) continue this motif. The four crossovers between the initial five parallel strands of the sheet are all helical, and the crossover chirality is the commonly observed right-handed form (22). β6 runs antiparallel to the adjacent β5 and β7. Thus all β-strands in this sheet

Table 1. Native, heavy-atom, and AsO_4^{3-} data for the GART crystal structure determination

Heavy-atom derivative data	Native	Derivative			
		MeHgOAc	*cis*Pt	$KAuCl_4$	AsO_4^{3-}
Resolution, Å	20.0–3.5	12.0–3.5	12.0–3.5	20.0–3.5	20.0–3.5
Refs. measured, no.	33791	41498	41549	29721	42254
Refs. unique, no.	8829	8720	8917	8803	9129
Refs. $F/\sigma > 2$, no.	8363	8364	8301	8122	8626
$\langle I/\sigma \rangle$	23.80	27.75	18.44	21.40	19.87
R_{merge}	5.86	5.60	7.09	6.65	5.25
R_{deriv}		18.26	13.53	19.54	13.00
Sites, no.		11	10	5	
$\langle \|\|F_P\| - \|F_{PH}\|\| \rangle$		34.67	24.67	35.61	
$\langle fh \rangle$		37.17	22.12	30.15	
$\langle fh/\varepsilon \rangle$		2.14	1.57	1.37	
R_{Cullis}		0.59	0.66	0.72	

$R_{merge} = \Sigma_h \Sigma_{i=1}^{N} |\bar{I}(h) - I(h)_i| / \Sigma_h \Sigma_{i=1}^{N} I(h)_i$, where $I(h)_i$ is the ith measurement of reflection h, and $\bar{I}(h)$ is the mean value of the N equivalent reflections. $R_{deriv} = \Sigma_h ||F_{PH}| - |F_P|| / \Sigma_h |F_P|$, where F_P and F_{PH} are structure amplitudes for native and derivative data. $\langle fh \rangle$ is the mean structure amplitude of the heavy atoms, and ε is the rms closure error for all reflections. $R_{Cullis} = \Sigma_h ||F_{PH} \pm F_P| - |F_{H(calc)}| / \Sigma_h |F_{PH} - F_P|$ for the centric data, where $F_{H(calc)}$ is the heavy-atom structure factor. Refs., reflections; deriv, derivative. *cis*Pt, *cis*-$Pt(NH_3)_2Cl_2$.

Table 2. Refinement statistics for the GART crystal structure determination

	Apo	Ternary
Resolution, Å	8.0–2.8	8.0–2.5
Crystals, no.	2	1
Refs. measured, no.	124304	69765
Refs. unique, no.	16623	28188
$\langle I/\sigma \rangle$	15.6	9.1
R_{merge}	7.4	12.3
Refs. $F/\sigma > 0.5$, no.	15431	25408
R_{model}	0.225	0.250
Distance deviations, Å	0.020	0.019
Angle deviations, °	4.1	3.5

$R_{model} = \Sigma_h||F_{obs}| - |F_{calc}||/\Sigma_h|F_{obs}|$. See legend to Table 1.

have the same polarity, except the antiparallel β6. The N-terminal β-strand (β1) of the sheet is one of the central strands, and the C-terminal strand (β7) is at the edge of the sheet. Following strand seven is a long, slightly bent helix of 27 residues (161–187). A nearly conserved proline, a residue that often introduces kinks when found in long helices (23), is located several residues after the bend. The C-terminal residues then extend into several short antiparallel strands, which are more exposed to the solvent than the primary sheet.

The location of the active site is shown in Fig. 2*b* with the substrate and inhibitor drawn as white bonds. The ligands interact with β4 and β5 at their C-terminal ends, residues from α1 and α6, and with the three loops in the region (between β4 and α4, between β5 and α5, and the loop containing Asp-144 between β6 and β7).

Apo–ternary comparison. Overall the ternary and two independent apo molecules are quite similar, with a root-mean-square deviation between 186 Cα atoms of 0.92 Å (apo–apo), 0.91 Å (apo–ternary), and 1.12 Å (apo–ternary). However, there are regions where the structures differ significantly, especially around the active site. The two most important active-site differences are displayed in Fig. 3. (*i*) The long loop 110–132 is disordered in both apo molecules and clearly seen in the ternary molecule, although even there it is less well ordered (main chain <B> = 33 Å^2) than the average main-chain atom (<B> = 26 Å^2). (*ii*) Structural variability also exists in the 142–144 loop, along with correlated movements at His-108. This difference may be particularly significant because Asp-144 is known as an important catalytic residue, as discussed below. In Fig. 3 differences are seen between the two apo molecules, as well as between the apo and ternary molecules. In one apo molecule, the loop is in a closed conformation with Asp-144 directed inward and forming a closely associated tetrad of conserved side chains (Asn-106, His-108, His-137, and Asp-144). In the other apo molecule, this loop is open with Asp-144 on the surface and more exposed to solvent. The density is well ordered in both molecules, and the differences are probably related to influences of symmetry-related molecules in the crystal. It is difficult to say which of these conformations, if either, would be the predominant apo structure in solution, but the closed conformation is less influenced by crystal-packing effects. These three molecules show the high degree of conformational flexibility that exists in this enzyme active site. This is an important consideration in understanding the reaction mechanism and in structure-based inhibitor design.

Substrate GAR-Binding Site. The location of the enzyme active site can be seen in Fig. 2*b*. The substrate GAR and the folate inhibitor bind adjacent to the fourth and fifth strands of the β-sheet, at the C-terminal end.

It was first postulated that this region was the active-site region from the apocrystal form. A significant piece of density off the side chain of Ser-12 was observed in both apo molecules. This density was thought due to a phosphate-binding site, where inorganic phosphate from the crystallization solution was bound and where the phosphate group of GAR would be located in a complex with substrate. A difference Fourier analysis between crystals soaked in AsO_4^{3-} and PO_4^{3-} revealed two large peaks at 15.5 σ and 14.7 σ, the

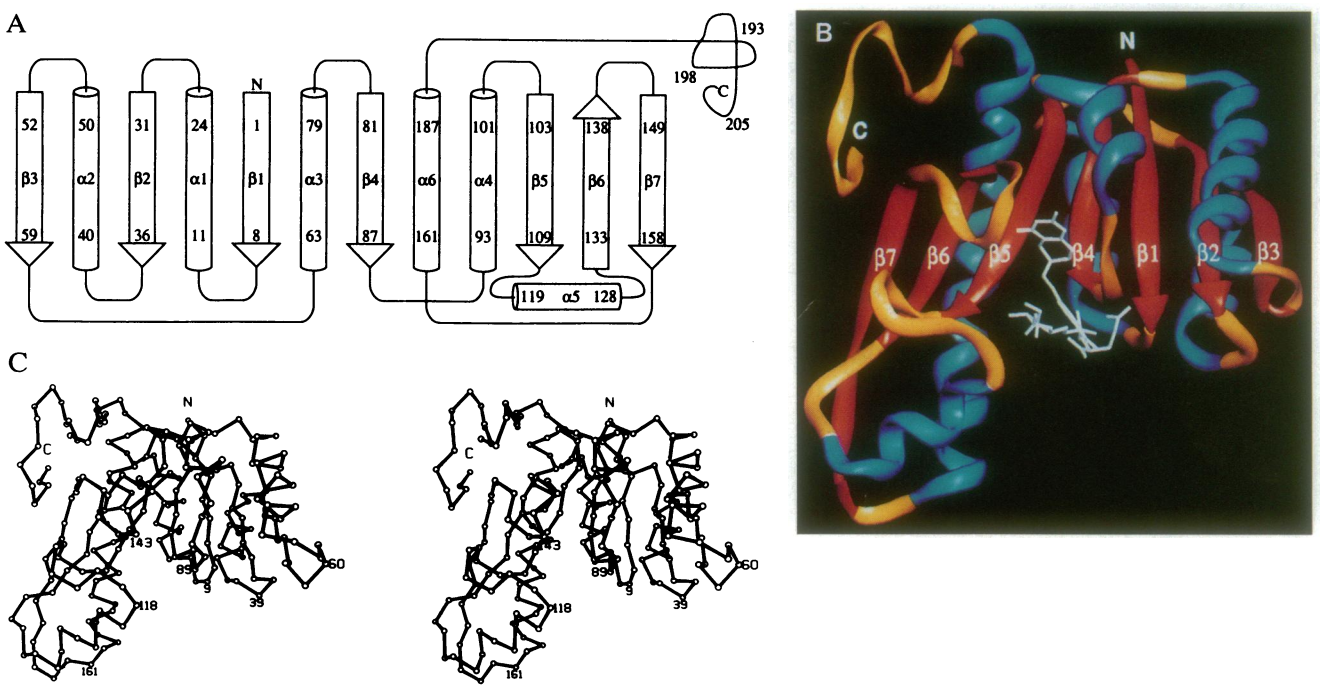

FIG. 2. (*A*) Topology of the secondary structural elements of GART. Arrows indicate β-sheet, and cylinders represent α-helices. The approximate beginning and ending residue numbers are given. (*B*) Ribbon drawing (18) of the C$^\alpha$ coordinates of ternary GART, showing the seven strands of β-sheet (red arrows), the six α-helices (blue), and coil (yellow). Binding sites for the substrate GAR and the inhibitor 5dTHF are seen as white bonds. (*C*) Stereo diagram of the C$^\alpha$ atoms of ternary GART in approximately the same orientation as *B*. Several residues are labeled, including the N- and C-terminal residues.

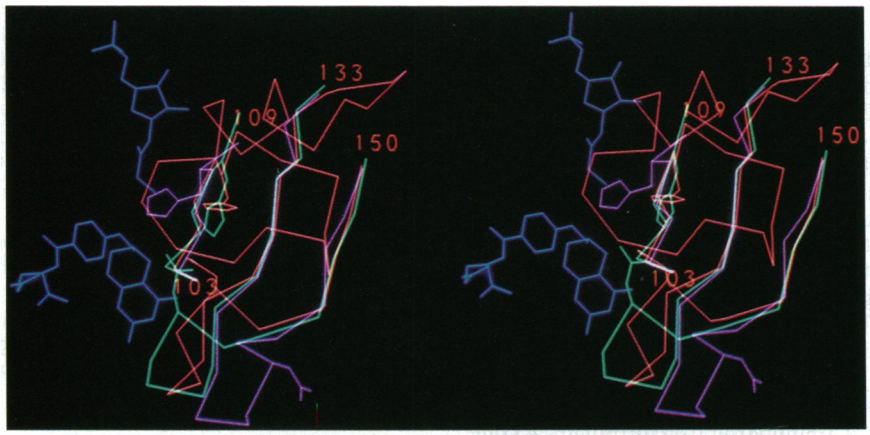

FIG. 3. Stereo view of portions of the two apo molecules (purple and blue-green; C^{α} atoms for residues 103–109 and 133–150) superimposed onto the ternary molecule (red; C^{α} atoms for residues 103–150). The side chains of His-108 and Asp-144 are shown for each molecule, as are the positions of substrate GAR and inhibitor 5dTHF (blue) in the ternary complex. Residues 110–132 are disordered in both apo molecules and ordered in the ternary molecule. The bicyclic ring of the inhibitor can be seen as too close to Asp-144 in the blue-green apo molecule, and this portion of the molecule must move to accommodate inhibitor binding. Likewise, it can be seen that His-108 in the purple apo molecule must move to allow GAR binding.

largest two peaks in the difference map, verifying that a single inorganic PO_4^{3-} is bound to each apo molecule. This phosphate-binding site is located between the end of the first β-strand and the N terminus of the subsequent helix in the β–α–β–α–β mononucleotide-binding domain. Phosphate binding using this type of secondary structure has been seen in a variety of nucleotide-binding proteins. This position along the loop between the β-strand and the α-helix is thought favorable due to its interactions with main-chain NH groups at the beginning of the helix and the favorable electrostatic interactions between the negative charge of the phosphate group and the dipole of the α1 helix (24). This area is the most highly conserved portion of GART, with 6 of the 12 residues (5–16) identical in six species (4).

The GAR-binding site observed in the ternary complex (Fig. 4) has the phosphate group located at the inorganic phosphate-binding site found in the apocrystal form. The terminal three oxygen atoms of the phosphate interact primarily with the main-chain NH groups of residues 11, 12, and 13, the γ-oxygen of Ser-12, and the δ-NH_2 of Asn-13. The fourth phosphate oxygen is within hydrogen-bonding distance of the ε-NH_2 of Gln-170. The 3-hydroxyl group from the ribose ring is within hydrogen-bonding distance of both the ε-NH_2 of Gln-170 and one side-chain oxygen of Glu-173. The 2-hydroxyl is hydrogen bonded to the other side-chain oxygen of Glu-173. Both residues 170 and 173 are part of the long α6-helix and are located near the proline bend.

Inhibitor-Binding Site. The inhibitor 5dTHF and its interactions within the protein active site are displayed in Fig. 4. The bicyclic portion of the inhibitor is well ordered, the benzoyl ring becomes less ordered, and the glutamate end is at the enzyme surface and is disordered. The orientation of the bicyclic ring is clear in the density maps with the 2-amino, 4-oxo, and bridge group at the 6 position being good markers. This ring is located with its surface over a volume of tightly packed hydrophobic residues. The edges of the ring are hydrogen bonded to main-chain atoms of the protein, which provides a rigid structure for binding, even though some of the hydrogen bonds are to atoms in the flexible loop containing Asp-144. Inhibitor hydrogen-bond acceptors include

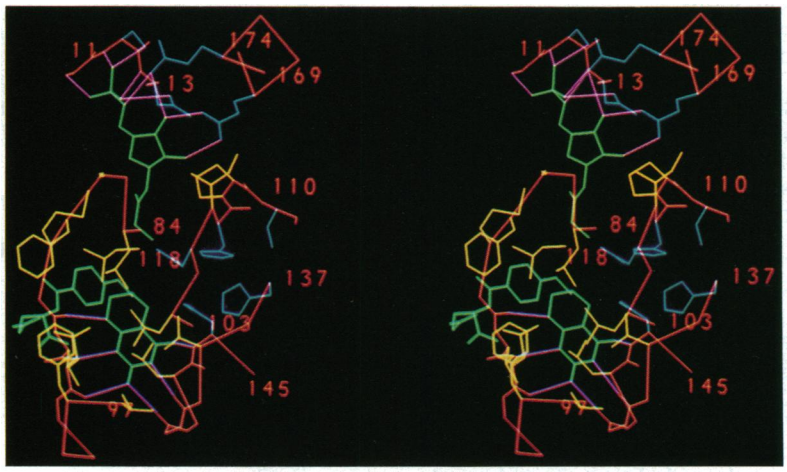

FIG. 4. Stereo view of the active site of GART, substrate GAR, and inhibitor 5dTHF (green). Selected main-chain atoms (11–13, 84–97, 103–110, 137–145, 169–174) are shown in red. Hydrophobic residues are shown in yellow. These include a hydrophobic base below the bicyclic ring (Leu-85, Phe-88, Leu-92, Phe-96, Val-97, Leu-104, Val-139), residues surrounding the benzoyl ring above the bicyclic ring (Met-89, Ile-91, Leu-118, Leu-143), and residues near GAR (Gly-87, Ile-107, Pro-109). Hydrophilic residues are shown in blue; these include five residues, which we propose will be near the formyl group of the substrate 10fTHF and may participate in catalysis (Asn-106, His-108, Ser-110, His-137, and Asp-144); also shown are five residues involved in GAR binding (Gly-11, Ser-12, Asn-13, Gln-170, Glu-173). Important hydrogen bonds ≤3.1 Å are shown as solid lines (purple). These include six to the bicyclic ring ($N^{1}\cdots92N$, $N^{2\alpha}\cdots92O$, $N^{2\alpha}\cdots141O$, $O^{4\alpha}\cdots144N$, $N^{8}\cdots90O$ and $N^{3}\cdots140O$) and nine to GAR (2OH···173$O^{\varepsilon 1}$, 3OH–173$O^{\varepsilon 2}$, 3OH···170$N^{\varepsilon 2}$, 5O···170$N^{\varepsilon 2}$, PO1···13N, PO1···13$O^{\delta 1}$, PO2···12N, PO2···12O^{γ}, and PO3···11N).

the ring N1 to the enzyme residue 92 NH group (92NH) and the 4-oxo to 144 NH; donors include the 2-NH_2 to 92O and 141O, N8 to 90O, and possibly N3 to 140O.

The ternary complex was formed with GAR and a mixture of 6(*R*) and 6(*S*)-5dTHF. Either or both isomers could bind, with the C6 substituent in either an axial or equatorial conformation. Given the bicyclic-ring orientation, the axial *S* inhibitor cannot bind because it would severely overlap protein atoms. The equatorial *R* and *S* isomers can fit into the active site, but do not fit the density as well as the axial *R* isomer shown in Fig. 4. This is the opposite C6 enantiomeric configuration of biologically reactive folates. The axial conformation is presumably the lower energy conformation since the solution conformation of tetrahydrofolate as determined by NMR has the C6 substituent axial (25). This chirality around C6 is the same found in the slightly more potent isomer of the inhibitor 5,10-dideazatetrahydrofolate, a compound very similar to 5dTHF, which inhibits murine GART with a K_i that is three times lower than the other isomer (1, 26). The benzoyl ring of the folate inhibitor is located in a channel of hydrophobic residues including Met-89, Ile-91, Leu-118, and Leu-143.

SAR. SAR for inhibitor binding to murine GART (1) have been studied. Although monofunctional *E. coli* GART is only ≈20% the size of this trifunctional mammalian enzyme, it is homologous with the C-terminal portion, and much of the SAR data should be explained with the *E. coli* structure (Fig. 4).

The postulated hydrogen bonding at N8 and at the 2-NH_2 group from SAR (1) is confirmed. The importance of CH_2 over NH at position 5 can also be seen. A NH group is more costly to desolvate upon binding, and there are no ligand–enzyme interactions to compensate. SAR data indicate π–π interactions with the benzoyl ring are not important: replacement of the phenyl ring with a cyclohexyl ring or methylene units retains activity. This result is explained by the finding that the benzoyl region interacts with the enzyme through saturated hydrophobic residues, where precise geometry is not critical for interactions and flexibility of these side chains can accommodate different inhibitors. Finally, the SAR data show the glutamate region does not contribute to binding. This result is consistent with the weak density and high-temperature factors for this part of the inhibitor. The nearby residues Arg-64 and Arg-90 may be important in the tighter binding of the polyglutamate forms.

Mechanistic Implications. The mechanism of GART is ordered-sequential: the folate substrate binds first, and the GAR binds second (27); the neutral amine is the reactive group (pH optimum 7.9–8.3). It is proposed that the reaction proceeds by direct nucleophilic attack by the amine of GAR on the formyl carbon of 10fTHF, forming a tetrahedral intermediate (28, 29). Asp-144 functions in a critical role during catalysis; its mutation to asparagine produces an inactive enzyme that still binds substrates (30).

The substrate 6(*R*)-10fTHF was modeled into the active site where there are three conserved residues (Asn-106, His-108, and Asp-144) positioned such that they can assist the reaction. The side chain of Asp-144 is positioned near the N10 of the folate but not close enough to and sterically blocked from the α-amine of GAR. It is more likely that His-108 $N^{\delta 1}$ (3.4 Å from the amine of GAR) accepts a proton from GAR, resulting from the nucleophilic attack. His-108 transfers this proton to Asp-144 directly or through the tetrahedral transition-state oxygen and then to N10 of the 10fTHF, allowing product release. These proton transfers would require only small movements in a region of the protein shown to be flexible. Asn-106 is close to the modeled formyl-binding site and may function in stabilizing the negatively charged oxygen of the tetrahedral intermediate, analogous to the role of Asn-155 in the oxyanion hole in subtilisin (31).

The structure of the pharmacologically interesting enzyme GART has been solved, and the positions of the substrate GAR and the inhibitor 5dTHF have been determined. From this information a reaction scheme is proposed, and earlier SAR work is discussed. The structure will be useful as a tool for designing better inhibitors and, because the human sequence is homologous, for structure-based drug design.

We thank Dr. Dave Matthews, Dr. Ward Smith, and Dr. Terry Jones for discussions and critical reading of the manuscript; Dr. Zdenek Hostomsky and Howard Tenenbaum for large-scale cell growth; and Eli Lilly chemists Dr. Homer Pearce, Dr. Chuan Shih, and Nicholas Bach for 5dTHF and GAR.

1. Baldwin, S. W., Tse, A., Gossett, L. S., Taylor, E. C., Rosowsky, A., Shih, C. & Moran, R. G. (1991) *Biochemistry* **30**, 1997–2006.
2. Taylor, E. C., Harrington, R. J., Fletcher, S. R., Beardsley, G. P. & Moran, R. G. (1985) *J. Med. Chem.* **28**, 914–921.
3. Beardsley, G. P., Moroson, B. A., Taylor, E. C. & Moran, R. G. (1989) *J. Biol. Chem.* **264**, 328–333.
4. Aimi, J., Qiu, H., Williams, J., Zalkin, H. & Dixon, J. E. (1990) *Nucleic Acids Res.* **18**, 6665–6672.
5. Smith, J. M. & Daum, H. A., III (1987) *J. Biol. Chem.* **262**, 10565–10569.
6. Saiki, R. K., Scharf, S., Faloona, F., Mullis, K. B., Horn, G. T., Erlich, H. A. & Arnheim, N. (1985) *Science* **230**, 1350–1354.
7. Tabor, S. & Richardson, C. C. (1985) *Proc. Natl. Acad. Sci. USA* **82**, 1074–1078.
8. Flensburg, J. & Skold, O. (1987) *Eur. J. Biochem.* **162**, 473–476.
9. Hostomsky, Z., Appelt, K. & Ogden, R. C. (1989) *Biochem. Biophys. Res. Commun.* **161**, 1056–1063.
10. Inglese, J., Johnson, D. L., Shiau, A., Smith, J. M. & Benkovic, S. J. (1990) *Biochemistry* **29**, 1436–1443.
11. Stura, E. A., Johnson, D. L., Inglese, J., Smith, J. M., Benkovic, S. J. & Wilson, I. A. (1989) *J. Biol. Chem.* **264**, 9703–9706.
12. Terwilliger, T. C. & Eisenberg, D. (1983) *Acta Crystallogr. Sect. A* **39**, 813–817.
13. Wang, B.-C. (1985) *Methods Enzymol.* **115**, 90–112.
14. Jones, T. A. (1978) *J. Appl. Crystallogr.* **11**, 268–272.
15. Yeates, T. O. & Rini, J. M. (1990) *Acta Crystallogr. Sect. A* **46**, 352–359.
16. Brunger, A. T. (1990) *Acta Crystallogr. Sect. A* **46**, 46–57.
17. Hendrickson, W. A. (1985) *Methods Enzymol.* **115**, 252–270.
18. Carson, M. (1991) *J. Appl. Crystallogr.* **24**, 958–961.
19. Richardson, J. S. (1981) *Adv. Protein Chem.* **34**, 167–338.
20. Rao, S. T. & Rossmann, M. G. (1973) *J. Mol. Biol.* **76**, 241–256.
21. Creighton, T. E. (1984) *Proteins* (Freeman, New York).
22. Richardson, J. S. (1976) *Proc. Natl. Acad. Sci. USA* **73**, 2619–2623.
23. Barlow, D. J. & Thornton, J. M. (1988) *J. Mol. Biol.* **201**, 601–619.
24. Schulz, G. E. & Schirmer, R. H. (1979) *Principles of Protein Structure* (Springer, New York).
25. Poe, M. & Benkovic, S. J. (1980) *Biochemistry* **19**, 4576–4582.
26. Moran, R. G., Baldwin, S. W., Taylor, E. C. & Shih, C. (1989) *J. Biol. Chem.* **264**, 21047–21051.
27. Caperelli, C. A. (1989) *J. Biol. Chem.* **264**, 5053–5057.
28. Smith, G. K., Mueller, W. T., Slieker, L. J., DeBrosse, C. W. & Benkovic, S. J. (1982) *Biochemistry* **21**, 2870–2874.
29. Caperelli, C. A. & McKellar, B. R. (1991) *Bioorg. Chem.* **19**, 40–52.
30. Inglese, J., Smith, J. M. & Benkovic, S. J. (1990) *Biochemistry* **29**, 6678–6687.
31. Takeuchi, Y., Satow, Y., Nakamura, K. T. & Mitsui, Y. (1991) *J. Mol. Biol.* **221**, 309–325.